Observation of the Parametric Two-Ion Decay Instability with Thomson Scattering

C. Niemann, S. H. Glenzer, J. Knight, L. Divol, E. A. Williams, G. Gregori, B. I. Cohen, C. Constantin, and D. H. Froula
Lawrence Livermore National Laboratory, 7000 East Avenue, Livermore, California 94550, USA

D. S. Montgomery and R. P. Johnson
Los Alamos National Laboratory, Los Alamos, New Mexico 87545, USA
(Received 8 October 2003; published 22 July 2004)

We present the first direct experimental observation of the parametric two-ion decay instability of ion-acoustic waves driven by a high intensity (5×10^{15} W cm^{-2}) laser beam in a laser produced high-Z plasma. Using two separate Thomson scattering diagnostics simultaneously, we directly measure the scattering from thermal ion-acoustic fluctuations, the primary ion waves that are driven to large amplitudes by the high intensity beam, and the two-ion decay products. The decay products are shown to be present only where the interaction takes place and their k spectrum is broad.

DOI: 10.1103/PhysRevLett.93.045004 PACS numbers: 52.35.Mw, 52.25.Os, 52.38.–r, 52.50.Jm

The nonlinear saturation of parametric instabilities, such as stimulated Brillouin scattering (SBS) plays a critical role for the energy coupling of laser light into large scale length plasmas for inertial confinement fusion (ICF). The SBS instability results from the resonant coupling of a high intensity laser pulse with an ion-acoustic wave to produce an electromagnetic wave scattered back from the plasma. It has been shown that SBS saturates for high laser intensities [1–4]. The two-ion decay, where a large amplitude ion-acoustic wave decays into two daughter waves, has been postulated as a saturation mechanism for SBS, particularly in medium- or high-Z plasmas [5–8]. Measurements of the two-ion decay instability [9] are important to improve our understanding of nonlinear plasma physics. Further, they allow the development of models [7] that will more precisely predict SBS laser energy losses in future laser facilities such as the National Ignition Facility (NIF).

In this Letter we present the first direct observation of the two-ion decay instability of SBS-driven ion-acoustic waves, driven in a gold (Au) plasma by a high intensity interaction beam (IB). Using two separate Thomson scattering (TS) diagnostics with different scattering geometries simultaneously, we directly measure the growth of the primary ion-acoustic waves driven by the IB, as well as the secondary two-ion wave decay products. Temporally, spectrally, and $\mathbf{k}$-vector resolved TS spectra of the decay products show both the scattering from thermal electrostatic fluctuations and the ion-acoustic waves excited to large amplitudes by the parametric decay instability.

The experiments were performed at the three beam Trident laser facility [10]. The Au plasma was created by a 200 J heater beam at 2ω (527 nm) in a 1.2 ns square pulse, focused onto a 1 mm $\times$ 400 μm, 50 μm thick Au foil using an $f/6$ lens. A strip line random phase plate (RPP) [11] produces a 1000×100 μm^2 line focus at the foil, delivering an intensity of 10^{14} W cm^{-2}. A second high intensity 2ω beam (50–200 J in a 1.2 ns square pulse) with a focal spot size of 80 μm and an intensity of up to 5×10^{15} W cm^{-2} was used as the IB. Propagating perpendicular to the heater beam and parallel to the Au foil, the IB drives ion-acoustic waves to large amplitudes, resulting in a SBS reflectivity of 5% (see also Ref. [12]). A third beam (1 J) at 3ω (351 nm) with a pulse length of 200 ps (FWHM) and a focal spot size of 250 μm (FWHM) serves as a low intensity TS probe beam [Fig. 1(a)]. The three beams are timed in such a way that the IB turns on 920 ps after the beginning of the heater beam and the probe beam is fired 400 ps after the beginning of the IB.

The SBS instability is a resonant three wave process between the incident electromagnetic wave $(\omega_{2\omega}, \mathbf{k}_{2\omega}) = (2\pi c/527\ \text{nm}, 2\pi/527\ \text{nm})$, an ion-acoustic wave $(\omega_{ia}, \mathbf{k}_{ia})$, and the backscattered electromagnetic wave

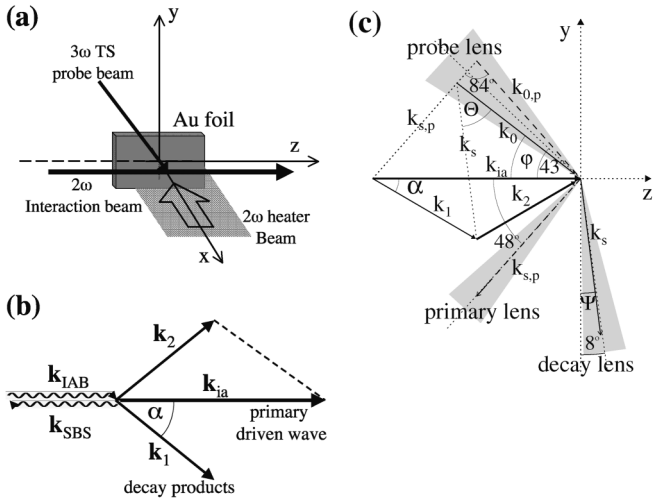

FIG. 1. (a) Experimental setup of the three Trident beams relative to the target foil, (b) schematics of the two-ion decay of a primary ion-acoustic wave into two daughter waves, and (c) scattering geometry of the two TS diagnostics to match the $\mathbf{k}$ vectors of the primary ion-acoustic wave $\mathbf{k}_{ia}$ and the two-ion decay product $\mathbf{k}_2$.

$(\omega_{2\omega} - \omega_{ia}, \mathbf{k}_{2\omega} - \mathbf{k}_{ia})$. Ion-acoustic waves driven by SBS propagate in the same direction as the IB with a k vector of $\mathbf{k}_{ia} \approx 2\mathbf{k}_{2\omega}$ [13]. These large amplitude primary waves can decay into two daughter waves, when the phase matching conditions $\mathbf{k}_{ia} = \mathbf{k}_1 + \mathbf{k}_2$, $\omega_{ia} = \omega_1 + \omega_2$ can be approximately satisfied [Fig. 1(b)]. We applied two separate TS diagnostics with different scattering geometries, to match the k vectors of the decay product and the primary driven wave simultaneously. To directly probe the two-ion decay products, we chose a scattering geometry, where the TS vector $\mathbf{k} = \mathbf{k}_s - \mathbf{k}_0$ matches the wave vector of one of the two decay products $\mathbf{k}_2$ ($\mathbf{k}_0$ and $\mathbf{k}_s$ are the wave vectors of the TS-probe beam and the scattered light, defined by the collection optics). The scattering geometry that fulfills this condition can be calculated from

$$\mathbf{k}_2 = \mathbf{k} = 2\mathbf{k}_0 \sin(\Theta/2), \quad (1)$$

where Θ is the scattering angle between incident and collected rays. Theory predicts that the two-ion decay is most probable with a finite decay angle α [7,8]. For example, with $\alpha = 30°$ (resulting from the calculations described below) we need an incident angle of $\varphi = 37°$ between the 2ω interaction and the 3ω probe beam, a scattering angle of $\Theta = 45°$ and a collection angle of $\Psi = 8°$ relative to the vertical [Fig. 1(c)]. To directly probe the primary ion-acoustic waves we need a scattering geometry with $\Theta = 84°$, $\varphi = 48°$, and $\Psi = -42°$ [Fig. 1(c)]. A single large aperture $f/2.5$ focusing lens, mounted at an intermediate angle of 43° relative to the IB allowed one to satisfy the matching conditions for both TS diagnostics with only one 3ω probe beam. The collection lenses for the decay and the primary wave diagnostics were mounted at angles of $\Psi = 8°$ and $\Psi = -42°$, respectively [Fig. 1(c)]. In order to cover a large range of $\mathbf{k}$ vectors we used fast $f/4$ achromatic collection lenses.

We performed the k-vector resolved TS measurements of the decay products by imaging the 24 mm diameter collection lens with an achromatic $f/10$ lens onto the slit of a 0.5 m imaging spectrometer (Chromex 500is), operating with a 1800 grooves/mm grating in the second order. The spectrometer was coupled to a gated, image intensified framing camera. The collection lens plane is imaged through the spectrometer onto the framing camera with spatial and spectral resolutions of 500 μm and 0.5 Å, respectively. The spectrometer slit selects a 125 μm wide region from the collection lens plane that lies within the y-z plane, parallel to the target foil.

The large aperture probe beam lens leads to an averaging of many different scattering angles for each Ψ, where the average TS angle varies along the lens from $\Theta = 46°$ for $\Psi = 1°$ to $\Theta = 32°$ for $\Psi = 15°$ ($\Theta = 47° - \Psi$). A 0.8 mm diameter pinhole in the image plane of the target chamber center (TCC) between the imaging lens and the spectrometer was used to define a $\varnothing$ 150×200 μm^3 small TS volume at TCC. The camera was gated with a minimum exposure time of 1.3 ns while the temporal resolution of the measurement was determined by the 200 ps pulse width of the 3ω probe beam. For the primary wave diagnostics we used an achromatic $f/9$ lens to image TCC onto the slit of a second 0.5 m imaging spectrometer coupled to a streak camera, yielding a temporal and spectral resolution of about 80 ps and 0.6 Å, respectively. The measurements were typically performed at a distance of $x = 300$ to 400 μm and $z = -200$ to -400 μm from TCC.

Figure 2(a) shows the $\mathbf{k}$-resolved two-ion decay measurements. We observe a strong asymmetry between the redshifted and the blueshifted peaks (I), due to collective scattering off ion-acoustic waves that are excited to large amplitudes by the two-ion decay instability. This observation is directly correlated with primary ion-acoustic

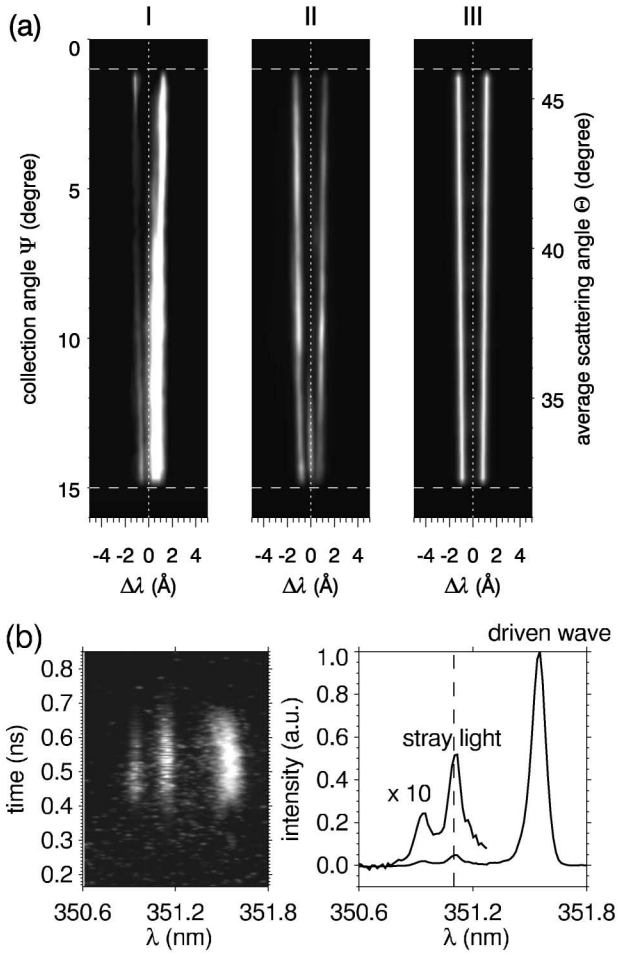

FIG. 2. (a) The $\mathbf{k}$-vector resolved two-ion decay measurement (I), thermal spectrum from a plasma region where no primary wave is driven (II), and a calculated $\mathbf{k}$-resolved thermal spectrum (III). The intensity asymmetry (I) is due to scattering off ion-acoustic waves stimulated by the two-ion decay instability. (b) Streaked spectrum from the primary wave diagnostic showing a strong enhancement of the redshifted SBS-driven peak, compared to the thermal blueshifted peak.

wave amplitudes, driven by SBS [Fig. 2(b)]. When no primary waves are driven inside the TS volume, we observe two symmetric thermal peaks (II). The separation of the two peaks increases with the average TS angle Θ. This increase is well reproduced in the calculated spectrum, where we assumed an electron temperature of 950 eV (III) [14].

The streaked TS spectrum from the primary wave diagnostic [Fig. 2(b)] is also dominated by the redshifted peak, due to collective scattering off the ion-acoustic waves that are excited to large amplitudes by SBS from the IB. The integrated intensity of the redshifted peak is 2 orders of magnitude higher than the blueshifted peak, the latter is due to thermal fluctuations. The central peak is caused by unshifted stray light from the TS-probe beam reflected from the edge of the foil.

Figure 3(a) shows lineouts of the driven and the undriven two-ion decay spectra. They indicate that the redshifted peak is about an order of magnitude larger than the blueshifted peak. In the pure thermal scattering case the two peaks are close to being symmetric as expected.

For our plasma conditions, the scattering parameter is $1/(|\mathbf{k}|\lambda_D) > 1$ and the scattering is collective ($\mathbf{k}$ is the thermal TS wave vector and λ_D the Debye length). The electron temperature can directly be determined from the separation of the two peaks in the ion feature if the charge state Z is known [14]. We assume an average charge state of $Z = 40$, which was measured in previous Trident experiments with identical target and beam parameters [12]. An electron density of 10^{20} cm^{-3} was calculated by radiation-hydrodynamic modeling and is consistent with other experiments [15]. The k-resolved TS spectra allow a very precise temperature determination of the order of a few percent, since the spectrum can be fit for each $\mathbf{k}$. Measured temperatures vary from 350 eV at a distance of $x = 450$ μm from the foil to more than 1 keV at a distance of $x = 200$ μm consistent with previous experiments [12]. This temperature gradient induces a 0.3 Å broadening of the thermal peaks in Fig. 3(a), which is smaller than the 0.5 Å spectral resolution of the instrument.

Primary ion-acoustic waves as well as two-ion decay products are observed only between $z = -200$ and -400 μm. Figure 3(b) shows the averaged intensity ratio between the redshifted and the blueshifted peaks as a function of transverse displacement Δx from the IB. The experiments clearly show that an asymmetry of the two

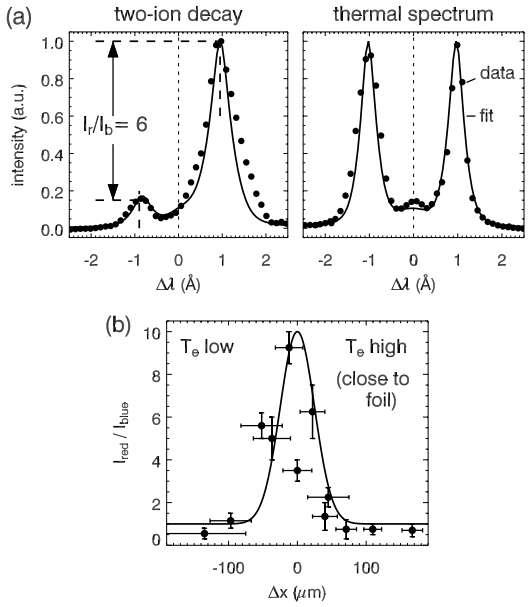

FIG. 3. (a) Comparison of the two-ion decay spectra for a shot where SBS drives ion-acoustic waves to large amplitudes and a shot where no waves are driven inside the TS volume. In the first case, light scatters directly from large amplitude ion-acoustic waves that were driven by the two-ion decay instability, and the redshifted peak is enhanced. The undriven spectrum shows two symmetric thermal peaks and the unshifted stray light as expected. (b) Averaged relative amplitude of the redshifted to the blueshifted peak intensity from the decay products as a function of transverse displacement Δx of the TS volume from the IB.

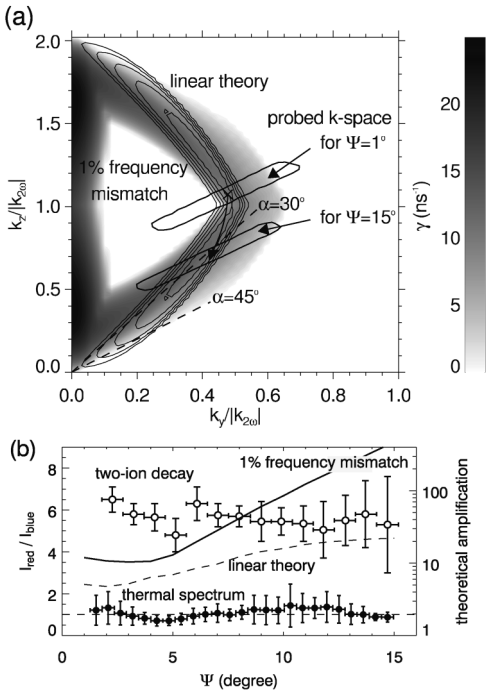

FIG. 4. (a) Two-ion decay growth rate γ as a function of decay vector coordinates k_y and k_z assuming pure linear theory [7] (contour) and a frequency mismatch of the primary wave of $\pm 1\%$ (color map). The primary wave is driven along k_z. The contours show the probed $\mathbf{k}$-vector space for the upper and lower edges of the lens ($\Psi = 1°$ and 15°). (b) Relative averaged amplitude of ion-acoustic waves excited by the two-ion decay instability (discrete points, linear scale) as a function of $\mathbf{k}$ (collection angle Ψ). The theoretical amplification assuming pure linear theory (dashed curve) and a frequency mismatch of the primary wave of 1% (solid line) are shown for comparison (log scale).

peak,s and thus the two-ion decay, is observed only when the IB volume and the TS volume overlap ($|\Delta x| \leq 50\,\mu$m), which demonstrates that the two-ion decay is correlated with the SBS driven ion-acoustic wave amplitude.

The two-ion decay instability differs from more familiar parametric instabilities, such as stimulated Brillouin and Raman scattering, in that the frequency and wave number matching condition $\omega(k_{ia}) = \omega(k) + \omega(k_{ia} - k)$ with $\omega(k) = c_s k/\sqrt{1 + k^2\lambda_D^2}$ cannot be exactly satisfied, except in the limit ($\lambda_D \to 0$) of zero dispersion [6]. However, in that limit, the anti-Stokes coupling to the ion wave with wave number $k_{ia} + k$ is also resonant, which stabilizes the potential instability. Instability thus results only for those wave numbers in which the Stokes coupling exceeds the anti-Stokes coupling and for primary ion wave amplitudes sufficient to overcome the inevitable frequency mismatch.

Figure 4(a) shows the two-ion decay growth rate λ calculated from the dispersion relation derived in Ref. [7]. The experimental plasma parameters were used, which leads to $k_{ia}\lambda_D = 0.35$, and it was assumed that a large amplitude acoustic wave ($\delta n/n \simeq 0.15$) is driven by SBS. Such an amplitude is well below the wave breaking limit and was observed in numerical simulations of SBS ($\delta n/n$ corresponds to the local peak amplitude, localized in both time and space). Two-ion decay with a decay angle of $\alpha = a\tan(k_y/k_z) \approx 30°$ is most probable, but γ remains large over a broad range of $\mathbf{k}$. To compare with Fig. 2(a), we calculate the amplification due to the instability as seen at a given Ψ. Figure 4(a) shows the k space that is probed by the decay diagnostics for two positions on the collection lens ($\Psi = 1°$ and $15°$). The range of angles is determined by the $f/2.5$ probe beam lens and a uniform angular distribution of the primary driven waves within the $f/6$ cone of the IB. A convolution of the two-ion decay wave amplification $\exp[(\gamma - \nu_L)t]^2$ with the normalized probed k space for each Ψ, where $t = 500$ ps is the delay between the probe beam and the IB, leads to the curve labeled linear theory in Fig. 4(b). The electron Landau damping for the decay products is $\nu_L \simeq 6\ \text{ns}^{-1}$. Figure 4(b) also shows the relative measured wave amplitude of the decay products (measured ratio of the redshifted peak to the blueshifted peak) in a spectrum where two-ion decay waves are present and are a pure thermal spectrum. In accordance with the measurement, the theory predicts a rather flat response of the decay wave amplitude to Ψ. Using a wave amplitude closer to the threshold for the two-ion wave decay for our parameters ($\delta n/n > 0.05$, $\gamma > \gamma_L$) also leads to a broad secondary-wave spectrum.

A related complication is that because the primary ion wave is driven by SBS, its frequency and wave number do not necessarily exactly satisfy the local linear ion-acoustic dispersion relation, either from nonlinearity or from the plasma being inhomogeneous along the direction of SBS amplification [15]. The spectrum of unstable decay modes is sensitive to small frequency shifts of the primary ion wave of order $k_{ia}^2\lambda_D^2$. If a frequency mismatch of the primary wave as small as $\pm 1\%$ with regard to the acoustic frequency is introduced, one-dimensional decays along the direction of the primary wave ($\mathbf{k}_z$) become possible [16] [Fig. 4(a), color map], but Fig. 4(b) shows that decay is still predicted to be present around $\alpha = 30°$. Assuming a larger $\pm 5\%$ frequency shift (which corresponds to a $\pm 10\%$ variation in T_e along the IB path [15]) leads to a similar geometry of the decay. As a consequence, a primary ion wave driven by SBS with only modest linewidth can be expected to decay into a relatively broad spectrum of ion waves as observed in the experiments.

In summary, we have directly observed ion-acoustic waves excited by the parametric two-ion decay instability. Using two TS diagnostics simultaneously we measured both the primary waves that are driven by SBS from a high-intensity IB to large amplitudes as well as the secondary decay products. We have shown that decay waves are observed only inside the IB volume where SBS driven waves are large. We show that secondary decays occur over a broad $\mathbf{k}$ space in accordance with the theory. Two-ion decay processes might thus be energetically important for the saturation of SBS in ICF relevant plasmas.

We acknowledge the efforts of the Trident laser crew: T. Hurry, T. Ortiz, R. Gonzales, N. Okamoto, and R. Perea. This work was performed under the auspices of the U.S. Department of Energy by the University of California Lawrence Livermore National Laboratory under Contract No. W-7405-ENG-48.

[1] A. Ng *et al.*, Phys. Rev. Lett. **42**, 307 (1979).
[2] C. E. Clayton *et al.*, Phys. Rev. Lett. **51**, 1656 (1983).
[3] J. E. Bernard and J. Meyer, Phys. Rev. Lett. **55**, 79 (1985).
[4] S. H. Glenzer *et al.*, Phys. Rev. Lett. **86**, 2565 (2001).
[5] W. L. Kruer, in *From Fusion to Light Surfing*, edited by Thomas Katsouleas (Addison-Wesley, Redwood City, CA, 1991).
[6] S. J. Karttunen *et al.*, Phys. Fluids **24**, 447 (1981).
[7] B. I. Cohen *et al.*, Phys. Plasmas **4**, 956 (1997).
[8] C. Riconda *et al.*, Phys. Scr. **T84**, 217 (2000).
[9] H. C. Bandulet *et al.*, in Proceedings of the International Conference on Fusion Sciences and Applications, 2003 (to be published).
[10] N. K. Moncur *et al.*, Appl. Opt. **34**, 4274 (1995).
[11] B. S. Bauer *et al.*, Phys. Rev. Lett. **74**, 3604 (1995).
[12] D. H. Froula *et al.*, Phys. Rev. Lett. **88**, 105003 (2002).
[13] W. L. Kruer, *The Physics of Laser Plasma Interactions* (Addison-Wesley, New York, 1988).
[14] S. H. Glenzer *et al.*, Phys. Plasmas **6**, 2117 (1999).
[15] D. H. Froula *et al.*, Phys. Rev. Lett. **90**, 155003 (2003).
[16] L. Divol *et al.*, Phys. Plasmas **10**, 1822 (2003).